

Testing the AGN Unification Model in the Infrared

C. Ramos Almeida^{1,2}, N. A. Levenson³, A. Alonso-Herrero^{4,5}, A. Asensio Ramos^{1,2}, J. M. Rodríguez Espinosa^{1,2}, A. M. Pérez García^{1,2}, C. Packham⁶, R. Mason⁷, J. T. Radomski³, and T. Díaz-Santos⁸

¹ Instituto de Astrofísica de Canarias, La Laguna, Tenerife, E-38205, Spain.

² Departamento de Astrofísica, Universidad de La Laguna, E-38205, Spain.

³ Gemini Observatory, Casilla 603, La Serena, Chile.

⁴ Instituto de Física de Cantabria, CSIC-UC, Santander, E-39005, Spain.

⁵ Augusto González Linares Senior Research Fellow.

⁶ Astronomy Department, University of Florida, Gainesville, FL 32611-2055, USA.

⁷ Gemini Observatory, Northern Operations Center, Hilo, HI 96720, USA.

⁸ Spitzer Science Center, Pasadena, CA 91125, USA.

E-mail: cra@iac.es

Abstract. We present near-to-mid-infrared spectral energy distributions (SEDs) for 21 Seyfert galaxies, using subarcsecond resolution imaging data. Our aim is to compare the properties Seyfert 1 (Sy1) and Seyfert 2 (Sy2) tori using clumpy torus models and a Bayesian approach to fit the infrared (IR) nuclear SEDs. These dusty tori have physical sizes smaller than 6 pc radius, as derived from our fits. Active galactic nuclei (AGN) unification schemes account for a variety of observational differences in terms of viewing geometry. However, we find evidence that strong unification may not hold, and that the immediate dusty surroundings of Sy1 and Sy2 nuclei are intrinsically different. The Type 2 tori studied here are broader, have more clumps, and these clumps have lower optical depths than those of Type 1 tori. The larger the covering factor of the torus, the smaller the probability of having direct view of the AGN, and vice-versa. In our sample, Sy2 tori have larger covering factors ($C_T=0.95\pm 0.02$) and smaller escape probabilities than those of Sy1 ($C_T=0.5\pm 0.1$). Thus, on the basis of the results presented here, the classification of a Seyfert galaxy may depend more on the intrinsic properties of the torus rather than on its mere inclination, in contradiction with the simplest unification model.

1. Introduction

The unified model for active galaxies [4] is based on the existence of a dusty toroidal structure surrounding the central region of AGN. This geometry of the obscuring material allows the central engines of Type 1 AGN to be seen directly, resulting in typical spectra with both narrow and broad emission lines, whereas in Type 2 AGN the broad-line region (BLR) is obscured.

Pioneering work in modelling the dusty torus [28, 27, 10, 8, 11] assumed a uniform dust density distribution, although from the start, [16] realized that smooth dust distributions cannot survive within the AGN vicinity. In order to solve the discrepancies between the observations and the predictions from smooth torus models, an intensive search for an alternative torus geometry has been carried out in the last decade. The clumpy dusty torus models [22, 23, 13, 34] propose that the dust is distributed in clumps, instead of homogeneously filling the torus volume, and they are making significant progress in accounting for the mid-IR (MIR) emission of AGNs [19, 21, 14, 25, 33, 31, 12, 1].

In this work, we report IR nuclear fluxes for a representative sample of nearby Seyfert galaxies, for which we estimate unresolved nuclear MIR fluxes. We compile near-IR (NIR) nuclear fluxes from the literature of similar resolution to construct nuclear SEDs for all the galaxies, and fit them with clumpy torus models, which we interpolate from the [22, 23] database. Table 1 summarizes key observational properties of the sources in the sample.

Table 1. Basic Galaxy Data.

Galaxy	Seyfert type	z	Distance (Mpc)	Scale (pc arcsec ⁻¹)	Telescope	Instrument	Filters	Resolution (arcsec)
NGC 1097	1	0.0042	19	92	Gemini-S	T-ReCS	Si-5, Qa	0.41, 0.52
NGC 1566	1	0.0050	20	97	Gemini-S	T-ReCS	Si-2, Qa	0.30, 0.53
NGC 6221	1	0.0050	18	87	Gemini-S	T-ReCS	Si-2, Qa	0.32, 0.55
NGC 7469	1	0.0163	65	315	Gemini-S	T-ReCS	Si-2, Qa	0.31, 0.55
NGC 3227	1.5	0.0039	17	82	Gemini-N	Michelle	N'	0.39
NGC 4151	1.5	0.0033	13	64	Gemini-N	OSCIR	N, IHW18	0.53, 0.58
NGC 6814	1.5	0.0052	21	102	Gemini-S	T-ReCS	Si-2, Qa	0.28, 0.53
NGC 1365	1.8	0.0055	18	107	CTIO 4m	OSCIR	N, IHW18	0.92, 1.03
NGC 2992	1.9	0.0077	31	149	Gemini-N	Michelle	N', Qa	0.32, 0.53
NGC 5506	1.9	0.0062	25	120	Gemini-N	Michelle	N', Qa	0.36, 0.51
Centaurus A	2	0.0018	3.5	17	Gemini-S	T-ReCS	Si-2, Qa	0.30, 0.53
Circinus	2	0.0014	4	20	Gemini-S	T-ReCS	Si-2, Qa	0.33, 0.55
IC 5063	2	0.0113	45	219	Gemini-S	T-ReCS	Si-2, Qa	0.40, 0.62
Mrk 573	2	0.0172	69	334	Gemini-S	T-ReCS	N, Qa	0.36, 0.54
NGC 1386	2	0.0029	11	56	Gemini-S	T-ReCS	N, Qa	0.31, 0.54
NGC 1808	2	0.0033	11	64	CTIO 4m	OSCIR	N, IHW18	0.94, 1.02
NGC 3081	2	0.0080	32	155	Gemini-S	T-ReCS	Si-2, Qa	0.30, 0.56
NGC 3281	2	0.0107	43	208	Gemini-S	T-ReCS	N, Qa	0.34, 0.58
NGC 4388	2	0.0084	34	163	Gemini-N	Michelle	N', Qa	0.34, 0.50
NGC 7172	2	0.0087	35	169	Gemini-S	T-ReCS	N	0.51
NGC 7582	2	0.0053	21	103	CTIO 4m	OSCIR	N, IHW18	0.76, 0.99

2. MIR Observations

Ground-based MIR high-angular resolution observations of 21 nearby active galaxies were carried out over the past years for a variety of science drivers. We make use of this archive of data in this paper. The first set of observations was obtained with the University of Florida MIR camera/spectrometer OSCIR at the 4 m Blanco Telescope at Cerro Tololo Inter-American Observatory (CTIO) and at the Gemini North Telescope. Another set of observations was performed with the MIR camera/spectrograph T-ReCS (Thermal-Region Camera Spectrograph) on the Gemini-South telescope. The last set was obtained with the MIR camera/spectrograph Michelle on the Gemini North Telescope (see Table 1). Observations of PSF and flux standard stars were made for each galaxy through the same filters. The PSF star images were employed to determine the unresolved (i.e., nuclear) component of each galaxy. For further details on the MIR observations of the whole sample we refer the reader to [33, 31].

3. SED Observational Properties

Using the MIR data described in Section 2 and NIR data of similar resolution compiled from the literature, we constructed subarcsecond resolution nuclear SEDs in the wavelength range from

~ 1 to $18 \mu\text{m}$ for the galaxies in Table 1. Figures 1 and 2 show the individual SEDs.

Using the highest resolution data only (≤ 0.55 arcsec) we constructed average Sy1 and Sy2 templates (see Figure 4 in [31]) and measured the $1.265\text{--}18.3 \mu\text{m}$ IR slope ($f_\nu \propto \nu^{-\alpha_{IR}}$) of the Sy1 template: $\alpha_{IR} = 1.7 \pm 0.3$, as well as the NIR ($\alpha_{NIR} = 1.6 \pm 0.2$) and MIR spectral indexes ($\alpha_{MIR} = 2.0 \pm 0.2$). A flat NIR slope indicates an important contribution of hot dust emission (up to $\sim 1000\text{--}1200$ K; [6]) that comes from the immediate vicinity of the AGN. The shape of the Sy2 mean SED is very steep ($\alpha_{IR} = 3.1 \pm 0.9$, $\alpha_{NIR} = 3.6 \pm 0.8$, and $\alpha_{MIR} = 2.0 \pm 0.2$) compared with those of the Type 1 Seyferts. In general, Sy2 have steeper $1\text{--}10 \mu\text{m}$ SEDs than Sy1 [9, 3, 2]. On the contrary, the MIR slope is the same for the Sy1 and Sy2 templates ($\alpha_{MIR} = 2.0 \pm 0.2$).

4. SED Modelling

The clumpy dusty torus models of Nenkova et al. (2002) hold that the dust surrounding the central engine of an AGN is distributed in clumps, instead of homogeneously filling the torus volume. The clumpy database now contains 1.2×10^6 models, calculated for a fine grid of model parameters. The inherent degeneracy between these parameters has to be taken into account when fitting the observables. To this end, we developed a Bayesian inference tool (BayesClumpy; [5]).

The priors for the model parameters are assumed to be truncated uniform distributions in the intervals reported in Table 2. Therefore, we give the same weight to all the values in each interval. Apart from the six parameters that characterize the models, there is an additional parameter that accounts for the vertical displacement required to match the fluxes of a chosen model to an observed SED. This vertical shift scales with the AGN bolometric luminosity (see Section 5).

Table 2. Clumpy Model Parameters and Considered Intervals

Parameter	Abbreviation	Interval
Width of the angular distribution of clouds	σ	$[15^\circ, 70^\circ]$
Radial extent of the torus	Y	$[5, 30]$
Number of clouds along the radial equatorial direction	N_0	$[1, 15]$
Power-law index of the radial density profile	q	$[0, 3]$
Inclination angle of the torus	i	$[0^\circ, 90^\circ]$
Optical depth per single cloud	τ_V	$[5, 150]$

The results of the fitting process of the IR SEDs with the interpolated version of the clumpy models of [22, 23] are the posterior distributions for the six free parameters that describe the models and the vertical shift. When the observed data introduce sufficient information into the fit, the resulting posteriors will clearly differ from the input uniform priors, either showing trends or being centered at certain values within the intervals considered.

We fitted the individual IR SEDs with BayesClumpy, modelling the torus emission and the direct AGN contribution (the latter as a broken power law). We also consider the IR extinction curve of [7] to take into account any possible foreground extinction from the host galaxy. Although the solutions to the Bayesian inference problem are the posterior distributions of each parameter, we can translate the results into corresponding spectra (see Figures 1 and 2). The solid lines correspond to the model described by the combination of parameters that maximizes their probability distributions (maximum-a-posteriori; MAP). Dashed lines represent the model computed with the median value of the probability distribution of each parameter.

Shaded regions indicate the range of models compatible with the 68% confidence interval for each parameter around the median.

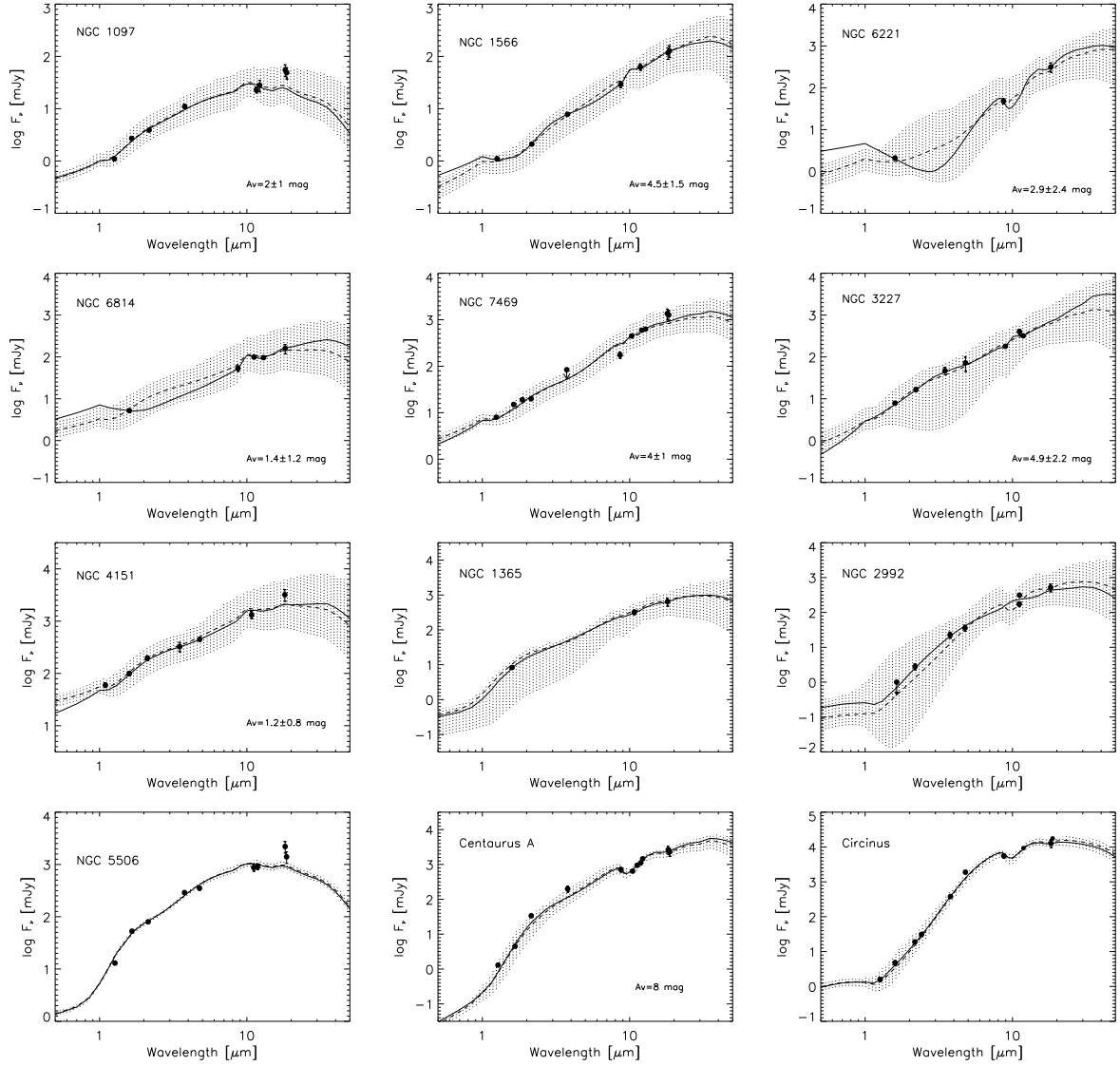


Figure 1. High spatial resolution IR SEDs of the Seyfert galaxies (dots). Solid and dashed lines correspond to the MAP and median models, respectively. Shaded regions indicate the range of models compatible with the 68% confidence interval for each parameter around the median.

The clumpy models successfully reproduce the observed Seyfert SEDs studied here with compatible results among them. This indicates that the NIR and MIR unresolved fluxes employed here are dominated by a combination of reprocessed emission from dust in the torus and direct AGN emission.

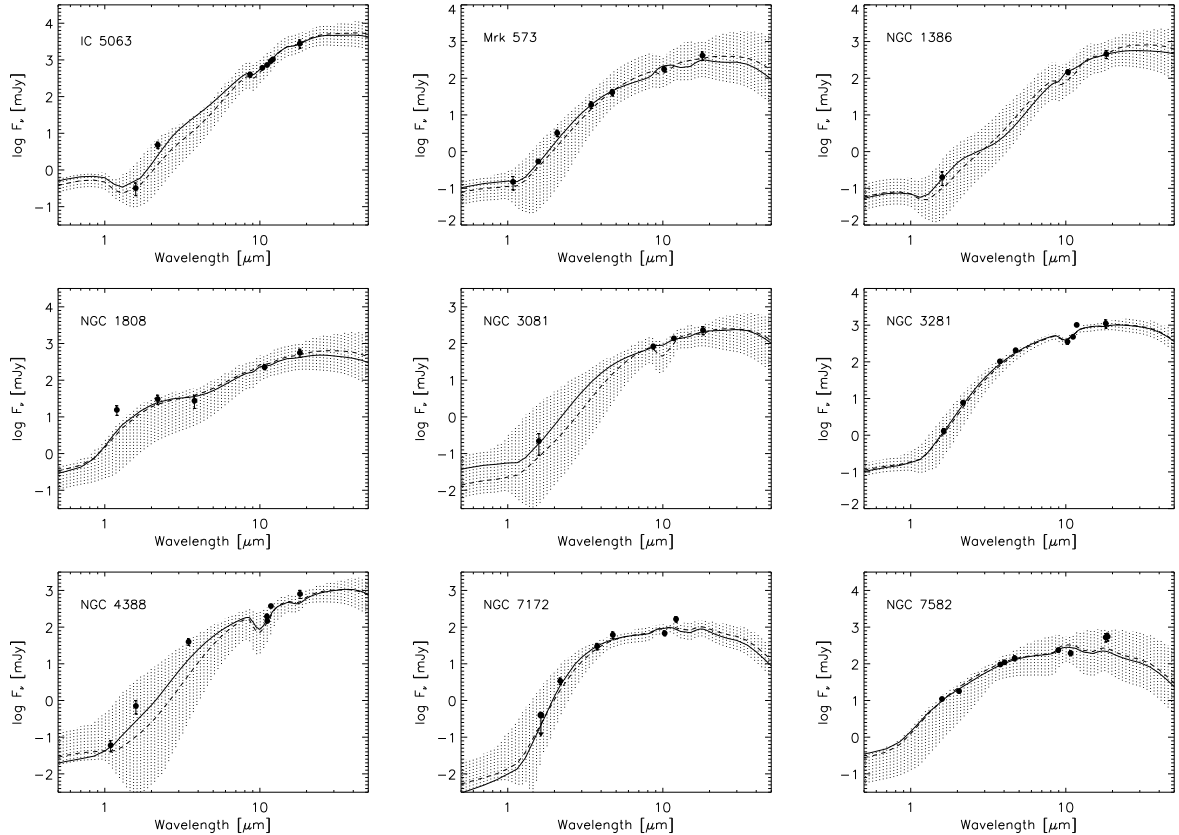


Figure 2. Same as in Figure 1, but for the remaining Sy2 galaxies.

5. Comparison between Type 1 and Type 2 Seyfert tori.

The aim of this work is to compare between the properties of Type 1 and 2 tori under the assumption that the SEDs studied here are torus/AGN dominated. Despite the relatively low number of objects considered (7 Sy1 and 9 Sy2; the unreliable fits of NGC 1808 and NGC 7582 are excluded), we find that some of the parameters are significantly different between Sy1 and Sy2.

To take full advantage of the Bayesian approach, the best way to compare the results for Sy1 and Sy2 galaxies is to derive joint posterior distributions for the full Type 1 and Type 2 datasets respectively. Thus, we normalized all the Sy1 SEDs at $8.74 \mu\text{m}$ and fitted them together using BayesClumpy, and we did the same for the Sy2. We considered the mean redshift for the Sy1 ($z=0.0061\pm 0.0045$) and for the Sy2 (0.0078 ± 0.0051) in the fits. In Figure 3 we show the Sy1 (left panel) and Sy2 fits (right panel). Note that the MAP and median models predict a flat SED with the silicate feature in weak emission for the Sy1 galaxies, and steeper and with the silicate band in shallow absorption for Sy2.

The comparison between the Sy1 and Sy2 posterior distributions is shown in Figure 4. From a visual inspection it is clear that the joint posteriors of the parameters N_0 , q , τ_V , and σ are completely different between Sy1 and Sy2. There is no overlap between the 1-sigma intervals. In Table 3 we report the median and mode values of the histograms in Figure 4.

In order to quantify how different the probability distributions are, we calculated the Kullback-Leibler divergence (KLD; [17]) between the Sy1 and Sy2 posteriors. This divergence takes into account the full shape of the posterior and it is a positive value, and equal to zero when two distributions are identical. Therefore, the larger the value of KLD, the more different

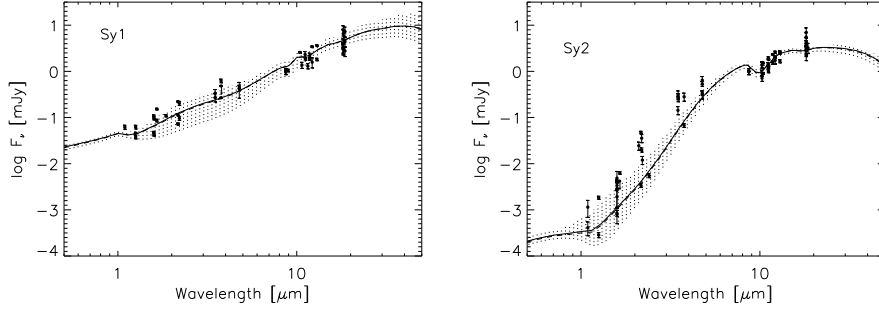


Figure 3. Same as in Figure 1, but for the Sy1 (left) and Sy2 SEDs (right) normalized at 8.74 μm .

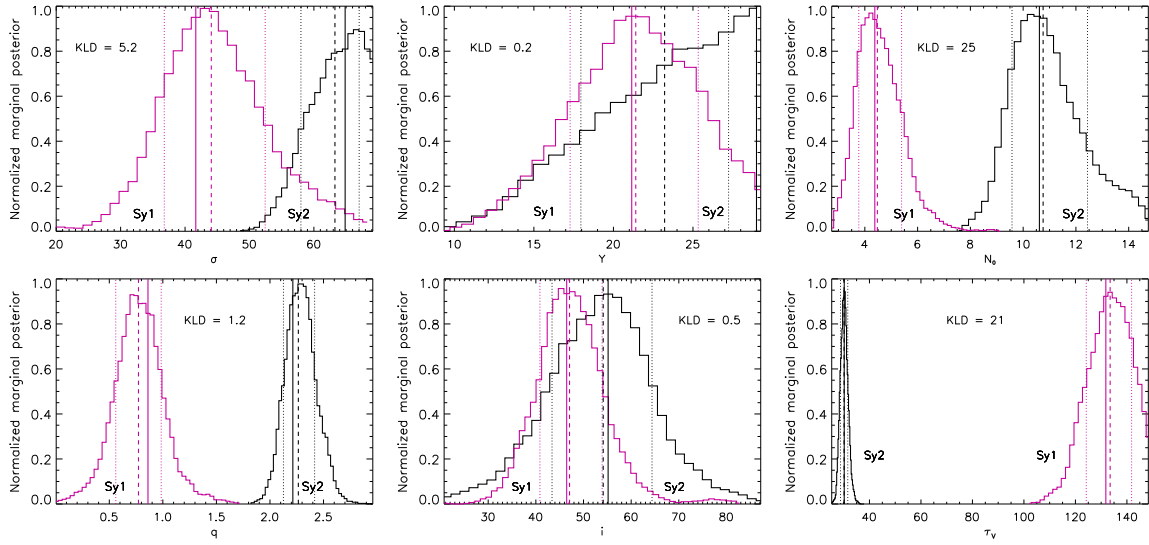


Figure 4. Posterior distributions resulting from the fits of the joint Sy1 and Sy2 SEDs. KLD values derived from the comparison between Sy1 and Sy2 for each parameter are labelled.

Table 3. Statistics of the comparison between Sy1 and Sy2 parameters

Type	σ (deg)		Y		N_0		q		i (deg)		τ_V	
	Sy1	Sy2	Sy1	Sy2	Sy1	Sy2	Sy1	Sy2	Sy1	Sy2	Sy1	Sy2
Medians	44 ± 8	63 ± 4	21 ± 4	23 ± 4	4 ± 1	11 ± 1	0.8 ± 0.2	2.3 ± 0.1	47 ± 7	54 ± 10	133 ± 8	30 ± 1
Modes	42	65	21	29	4	11	0.9	2.2	46	55	132	30

the posteriors. We find $\text{KLD} > 1$ for σ , N_0 , q , and τ_V (see Figure 4). These are indeed the four parameters whose 1-sigma regions do not overlap. Thus, we consider their differences significant between Sy1 and Sy2. For both Y and i we find $\text{KLD} < 1$ and similar median values between Sy1 and Sy2.

Sy1 tori are narrower and have fewer clouds ($\sigma = 44^\circ \pm 8^\circ$; $N_0 = 4 \pm 1$) than those of Sy2 ($\sigma = 63^\circ \pm 4^\circ$; $N_0 = 11 \pm 1$). The radial density distribution of the clouds is also different between the two Seyfert types according to this analysis: in Sy2, the majority of the clumps are distributed very close to the nucleus (i.e. steep radial density distribution; $q = 2.3 \pm 0.1$) whereas for Sy1 the clouds distribution is flatter ($q = 0.8 \pm 0.2$). On the other hand, the optical depth of the clouds in Sy1 tori is larger ($\tau_V = 133 \pm 8$) than in Sy2 ($\tau_V = 30 \pm 1$).

Interestingly, we find high as well as low values of the inclination angle of the torus for Sy1 and Sy2 (see Table 3). This variety in the i values translates into the similar median values of the joint Sy1 and Sy2 posteriors ($47^\circ \pm 7^\circ$ for Sy1 and $54^\circ \pm 11^\circ$ for Sy2), which are intermediate within the considered prior ($i=[0^\circ, 90^\circ]$). *This is telling us that, in the clumpy torus scenario, the classification of a Seyfert galaxy as a Type 1 or 2 may depend on the intrinsic properties of the torus rather than in mere inclination.*

In Figure 5 we represent the median values of σ and N_0 for the different Seyfert types over the covering factor contours. The covering factor is defined as $C_T = 1 - \int e^{-N_{LOS}(i)} d\cos(i)$. Type 1 nuclei tend to be located within lower C_T contours ($C_T \leq 0.6$) than those of Type 2s, for which $C_T \geq 0.5$, with the exceptions of Centaurus A and Mrk 573. We have represented with larger symbols the median values from the joint σ and N_0 posteriors reported in Table 3.

Since the covering factor is a non-linear function of the torus parameters, we took full advantage of our Bayesian approach and generated joint posterior distributions for C_T from those in Figure 4. The median values of the histograms are $C_T(\text{Sy2})=0.95 \pm 0.02$ and $C_T(\text{Sy1})=0.5 \pm 0.1$. The divergence between the Sy1 and Sy2 C_T posteriors is $\text{KLD}=28$, indicating that the difference is significant (1-sigma regions do not overlap). Thus, Sy1 tori in our sample have lower C_T s than those of Sy2, implying that they are intrinsically different.

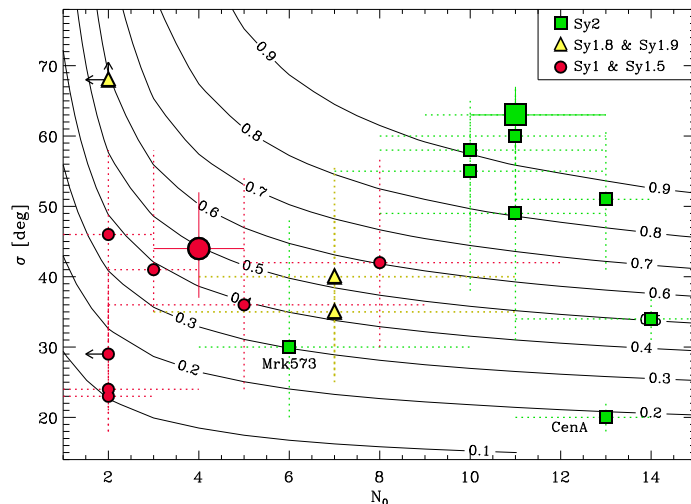


Figure 5. σ versus N_0 for the individual galaxies. Either median values or upper/lower limits are taken from the fits presented here. Error bars indicate 68% confidence level around the median. The big dot and square correspond to the average σ and N_0 values for Sy1 and Sy2 from Table 3.

The clumpy model fits yield the intrinsic bolometric luminosity of AGN (L_{bol}^{AGN}) by means of the vertical shift applied to match the observational data points. Combining this value with the torus luminosity (L_{bol}^{tor}), obtained by integrating the corresponding model torus emission (without the AGN contribution), we derive the reprocessing efficiency (RE) of the torus ($L_{bol}^{tor}/L_{bol}^{AGN}$). The previous values are calculated on the Bayesian framework, by combining the posterior distributions of the model parameters. Sy2 tori in our sample are more efficient reprocessors than Sy1, absorbing and re-emitting the majority of the intrinsic AGN luminosity in the IR: $\text{RE}(\text{Sy2})=[0.4, 1.0]$, with a median value of 0.8 and $\text{RE}(\text{Sy1})=[0.2, 0.7]$, with median of 0.5.

We considered a possible dependency of the RE (or alternatively the covering factor; C_T) on L_{bol}^{AGN} , since the amount of incoming radiation from the AGN could possibly have some influence on the reprocessed energy or even in the torus properties (e.g., receding torus scenario; [18]). However, we find no relationship between the two quantities in the luminosity range considered.

This means that the reprocessing efficiency depends primarily on the total number of clouds available to absorb the incident radiation, i.e. on the torus covering factor. However, the possible dependence of the torus properties on the AGN luminosity considering a broader luminosity range is further investigated in [1].

In general, the IR SED fitting does not constrain the size of the torus (Y) as well as other model parameters (see Section 5.3 in [33]). The NIR and MIR observations are sensitive to the warm dust (located within ~ 10 pc of the nucleus), which depends on the combination of model parameters N_0 , q , and Y [35]. Far-IR observations are more sensitive to the torus extent independently, as shown in [32]. The outer size of the torus scales with the AGN bolometric luminosity: $R_o = Y R_d$, so assuming a dust sublimation temperature of 1500 K, $R_o = 0.4 Y (L_{bol}^{AGN}/10^{45})^{0.5}$ pc. We derived R_o posterior distributions from those of L_{bol}^{AGN} and Y and find that all tori in our sample have outer radii smaller than 6 pc, in agreement with MIR direct imaging of nearby Seyferts [26, 30] and also interferometric observations [15, 36, 20, 29].

Summarizing, we find tantalizing evidence, albeit for a small sample of Seyfert galaxies and under the clumpy torus hypothesis, that the classification as a Type 1 and Type 2 depends on the intrinsic torus properties, in contradiction with the simplest unification model.

References

- [1] Alonso-Herrero, A., et al. 2011, ApJ, 736, 82
- [2] Alonso-Herrero, A., Quillen, A. C., Rieke, G. H., Ivanov, V. D., & Efstathiou, A. 2003, AJ, 126, 81
- [3] Alonso-Herrero, A., Quillen, A. C., Simpson, C., Efstathiou, A., & Ward, M. J. 2001, AJ, 121, 1369
- [4] Antonucci, R. R. J. 1993, ARA&A, 31, 473
- [5] Asensio Ramos, A. & Ramos Almeida, C. 2009, ApJ, 696, 2075
- [6] Barvainis, R. 1987, ApJ, 320, 537
- [7] Chiar, J. E. & Tielens, A. G. G. M. 2006, ApJ, 637, 774
- [8] Efstathiou, A., & Rowan-Robinson, M. 1995, MNRAS, 273, 649
- [9] Fadda, D., Giuricin, G., Granato, G. L., & Vecchies, D. 1998, ApJ, 496, 117
- [10] Granato, G. L., & Danese, L. 1994, MNRAS, 268, 235
- [11] Granato, G. L., Danese, L., & Franceschini, A. 1997, ApJ, 486, 147
- [12] Hönig, S. F., et al. 2010, A&A, 515, 23
- [13] Hönig, S. F., Beckert, T., Ohnaka, K., & Weigelt, G. 2006, A&A, 452, 459
- [14] Horst, H., Duschl, W. J., Gandhi, P., & Smette, A. 2009, A&A, 495, 137
- [15] Jaffe, W., et al. 2004, Nature, 429, 47
- [16] Krolik, J. H. & Begelman, M. C. 1988, ApJ, 329, 702
- [17] Kullback, S., & Leibler, A. 1951, Annals Math. Stat., 22, 79
- [18] Lawrence, A. 1991, MNRAS, 252, 586
- [19] Mason, R. E., et al. 2006, ApJ, 640, 612
- [20] Meisenheimer, K., et al. 2007, A&A, 471, 453
- [21] Mor, R., Netzer, H., & Elitzur, M. 2009, ApJ, 705, 298
- [22] Nenkova, M., Sirocky, M. M., Ivezić, Ž., & Elitzur, M. 2008, Ap
- [23] Nenkova, M., Sirocky, M. M., Nikutta, R., Ivezić, Ž., & Elitzur, M. 2008, ApJ, 685, 160
- [24] Nenkova, M., Ivezić, Ž., & Elitzur, M., 2002, ApJ, 570, 9
- [25] Nikutta, R., Elitzur, M., & Lacy, M. 2009, ApJ, 707, 1550
- [26] Packham, C., Radomski, J. T., Roche, P. F., Aitken, D. K., Perlman, E., Alonso-Herrero, A., Colina, L., & Telesco, C. M. 2005, ApJ, 618, L17
- [27] Pier, E. A., & Krolik, J. H. 1993, ApJ, 418, 673
- [28] Pier, E. A., & Krolik, J. H. 1992, ApJ, 401, 99
- [29] Raban, D., Jaffe, W., Röttgering, H., Meisenheimer, K., & Tristram, K. 2009, MNRAS, 394, 1325
- [30] Radomski, J. T., et al. 2008, ApJ, 681, 141
- [31] Ramos Almeida, C., et al. 2011a, ApJ, 731, 92
- [32] Ramos Almeida, C., et al. 2011b, MNRAS, 417, L46
- [33] Ramos Almeida, C., et al. 2009, ApJ, 702, 1127
- [34] Schartmann, M., et al. 2008, A&A, 482, 67
- [35] Thompson, G. D., Levenson, N. A., Uddin, S. A., & Sirocky, M. M. 2009, ApJ, 697, 182
- [36] Tristram, K. R. W., et al. 2007, A&A, 474, 837